minerals

Article

# Stratigraphic Section and Geochronological Studies of the Shoushan Basin, Fujian Province, South China, and Its Implications for the Mineralization of Shoushan Stone

**Yu-Juan Li [1,2], Lü-Yun Zhu [1,2,*], Wen Xu [1], Wei Meng [1], Min Lin [2], Zhong Yang [2] and Run-Sheng Chen [2]**

[1] Zijin School of Geology and Mining, Fuzhou University, Fuzhou 350108, China
[2] Fujian Provincial Institute of Geological Survey and Research, Fuzhou 350013, China
[*] Correspondence: zhulvyun@fzu.edu.cn or zhulvyun@126.com; Tel.: +86-1885-035-7676

**Abstract:** As one of the most famous craft-carving stones in China, Shoushan stone commonly consists of clay minerals, including the kaolinite, pyrophyllite, or illite group, which is the product of hydrothermal alteration. In Fujian Province, the Xiaoxi Formation of the Early Cretaceous is a critical formation containing pyrophyllite deposits (including Shoushan stone). Here, we carry out a geological field investigation of a typical section in the Shoushan basin of southeastern China to identify lithology and volcanic sequences of the Xiaoxi Formation. The section included four lithofacies: eruption facies, flood lava facies, sedimentary facies, and volcanic channel facies. The petrogenesis of these lithofacies demonstrates the evolution of volcanism, which is critical for understanding the formation of the Shoushan-stone-associated hydrothermal system. For the geochronological study, the samples of unaltered rhyolitic tuff are collected from the layers topping and bottoming a pyrophyllite orebody. The zircon U-Pb dating results constrain the age of pyrophyllite alteration during the episodic eruption. Shoushan stone is formed in an epithermal hydrothermal environment, so we suggest that high-quality Shoushan stone is formed by the hydrothermal alterations in the interval time of the volcanic episode (135–131 Ma) and after volcanic activity (<131 Ma). Furthermore, the Shoushan basin's stratigraphic section suggests that there have been large-scale hydrothermal systems in the volcanic basin during the Early Cretaceous volcanism. The stratigraphic correlation and geochemical results indicate that the Mesozoic basins in the Fu'an-Yongtai volcanic eruption belt have the potential for pyrophyllite deposit exploration.

**Keywords:** Shoushan stone; stratigraphic section; volcanic lithofacies; stratigraphic correlation; zircon U-Pb dating; mineralization age



**Citation:** Li, Y.-J.; Zhu, L.-Y.; Xu, W.; Meng, W.; Lin, M.; Yang, Z.; Chen, R.-S. Stratigraphic Section and Geochronological Studies of the Shoushan Basin, Fujian Province, South China, and Its Implications for the Mineralization of Shoushan Stone. *Minerals* **2022**, *12*, 1542. https://doi.org/10.3390/min12121542

Academic Editors: Andy H. Shen, Chaowen Wang, Bo Xu and Santanu Banerjee

Received: 5 October 2022
Accepted: 25 November 2022
Published: 30 November 2022



## 1. Introduction

Shoushan stone, one of China's most famous craft-carving stones (Figure 1), is mainly produced in the Shoushan basin in northern Fuzhou City, Fujian Province [1,2]. Shoushan stone can be divided into four main categories, including the Tianhuang stone, Gaoshan stone, hibiscus stone, and Wenyang stone based on their production places [2]. Significantly, the stone produced along the Shoushan river, also named Tianhuang stone (Figure 1b), is honored as the "emperor of Shoushan stone" due to its great cultural and economic values [3–7]. In gemology, Shoushan stone is classified as a colored gemstone. However, its common names are very complicated [8–10], which have been identified in more than 100 varieties by traditional custom [11].

Despite its complicated varieties, the mineral composition of Shoushan stone mainly includes kaolinite (e.g., kaolinite, dickite, nacrite), pyrophyllite, and illite group minerals [12–16]. These clay minerals are the product of the hydrothermal alteration of felsic magmatic rocks in common [8,9,11]. The Shoushan basin is a part of the Coastal Volcanic Belt in southeastern China. Significant volcanic activity during Late Mesozoic provided heat and hydrothermal fluids for alteration [17–19]. In theory, Shoushan stone is formed in an epithermal hydrothermal environment (100–405 °C) [20,21]. It is difficult to obtain accurate syngenetic age results, so the exact age limits for the Shoushan stone formation remain uncertain. Studies have demonstrated that the Xiaoxi Formation of the Early Cretaceous is a critical formation containing nonmetallic deposits, such as pyrophyllite and alum (including Shoushan stone) [22–25]. Our study chose a caldera (Qishan) in the Shoushan basin as a typical section to identify volcanic sequences and lithofacies. According to the stratigraphic correlation from the Early Cretaceous in Fujian Province, samples from the Xiaoxi Formation at different locations are collected to obtain their chemical compositions. Combined with the geochemical results, the geological background is revealed to understand the formation mechanism of Shoushan stone. The Xiaoxi Formation is composed of altered and unaltered volcanic rocks. Based on the result of a stratigraphic section, the mineralization (i.e., alteration) age of Shoushan stone is constrained by the magmatic zircon U-Pb age (135 and 131 Ma) of the critical host tuff.

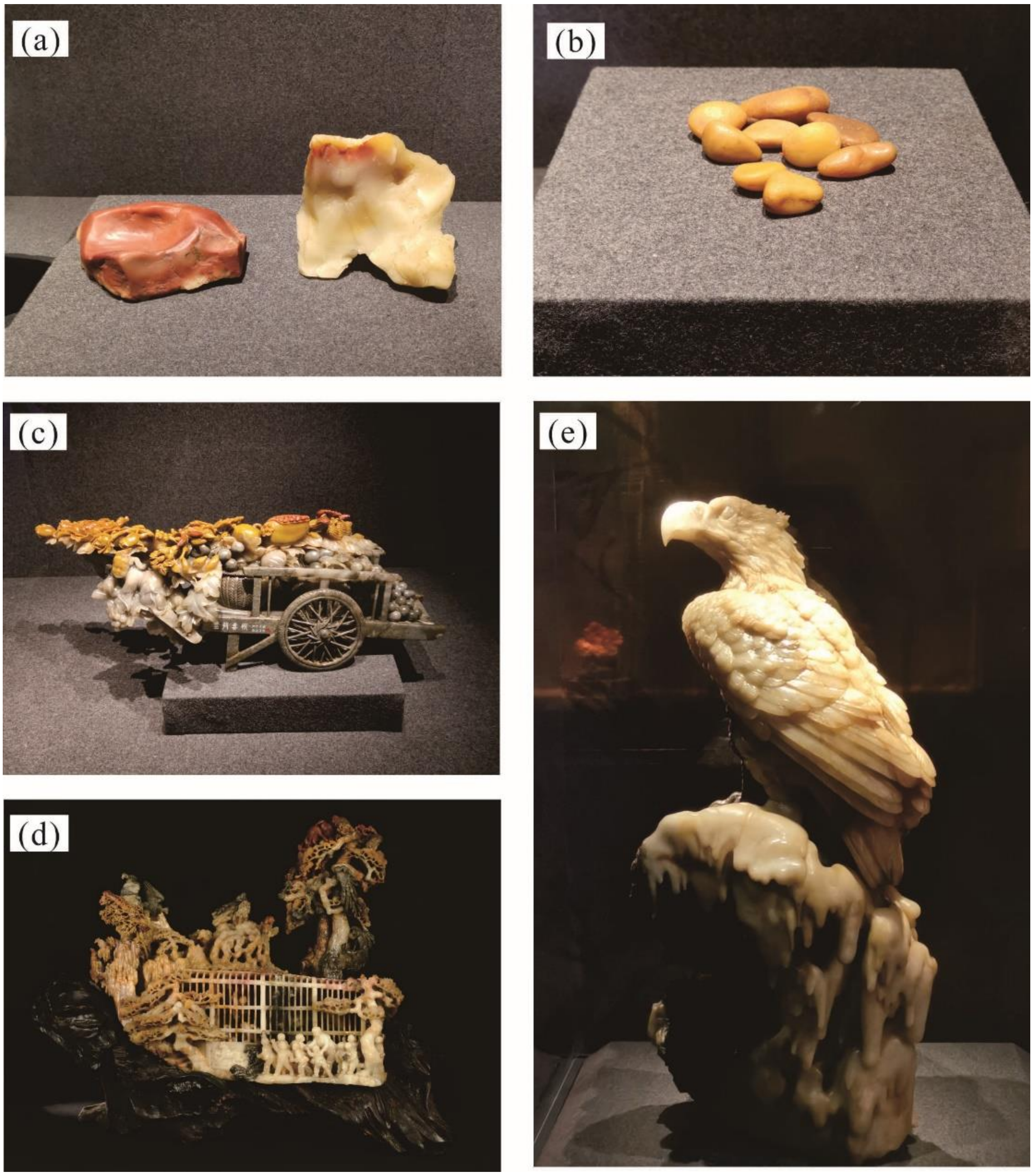


**Figure 1.** (**a**,**b**) Typical raw gemstone; (**b**–**e**) arts and crafts in China Shoushan Stone Museum.

## 2. Geologic Setting

Eastern China is formed by the collision of the North and South China Blocks along the Qinling–Dabie–Sulu Orogen during the Indosinian Period (Late Permian to Triassic) [26,27]. As shown in Figure 2a, the South China Block is separated by the northeast–southwest trending Jiangshan–Shaoxing Fault into the Yangtze Block and the Cathaysia Block [28]. During the Mesozoic (especially Jurassic and Cretaceous), there were massive volcano-intrusive emplacements in the Cathaysia Block, which shows a belt distribution within the coastal area between the Zhenghe-Dapu fault and Changle-Nan'ao fault in Fujian Province (Figure 2b) [29,30]. This coastal Mesozoic volcanic belt is generally dominated by acidic volcanic rocks, in contrast to the small content of intermediate-mafic volcanic rocks [29,31]. The Late Mesozoic volcanism in Fujian Province occurs in three cycles: 150–137 Ma for the Nanyuan Formation, 135–125 Ma for the Xiaoxi Formation, and 110–99 Ma for the Shimaoshan Group, all of which are the records of volcanism climax [22,25,32].

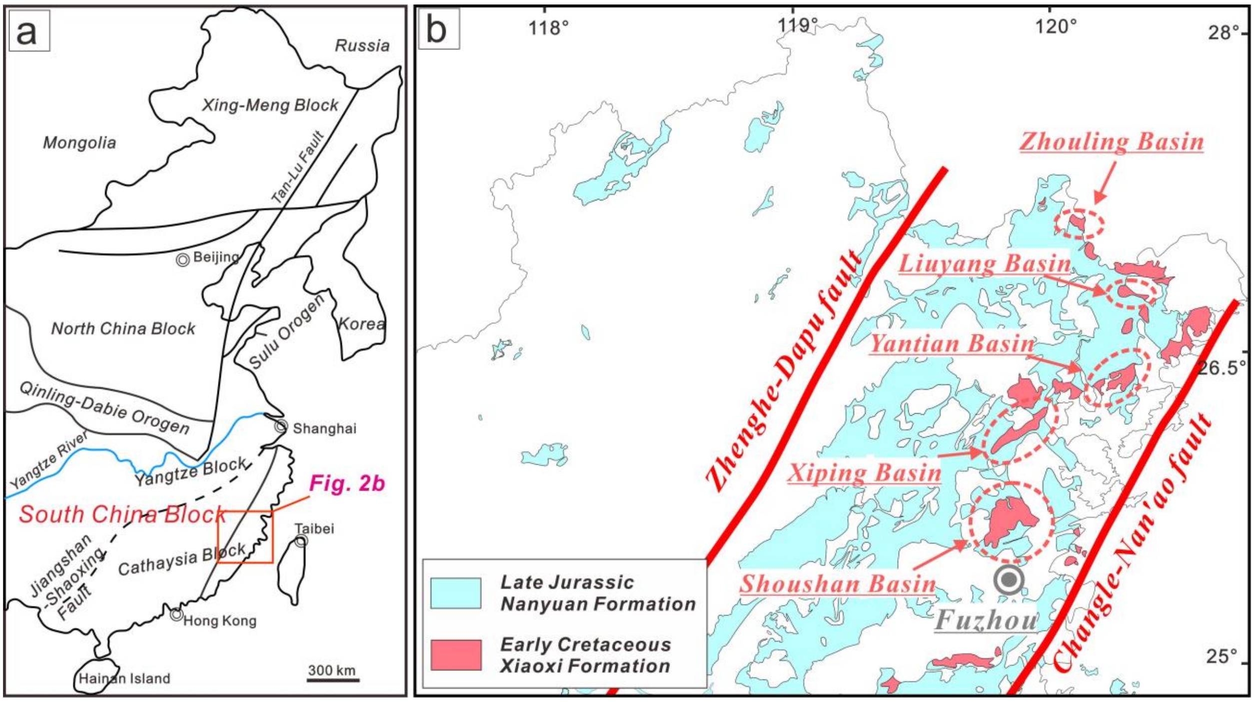


**Figure 2.** (**a**) Schematic map of geotectonic units in eastern China. (**b**) Schematic map of the Late Jurassic Nanyuan Formation and Early Cretaceous Xiaoxi Formation in Southeastern Fujian Province.

The Shoushan basin, as a representative of these Mesozoic volcanic basins, is mainly composed of the Early Cretaceous Xiaoxi Formation, which overlies the Late Jurassic Nanyuan Formation (Figure 3). Due to the epithermal hydrothermal alteration, some layers of the Xiaoxi Formation contain several large-scale nonmetallic deposits, including pyrophyllite for industry and Shoushan stone for craft carving [23]. For example, the cumulative identified reserves of industrial-grade pyrophyllite are more than 12.48 million tons in the Emei and Shoushan mining areas [24]. As Figure 3 shows, there are several volcanic eruption centers or reactivated calderas (e.g., Shoushan, Qishan, Gaoshan, Furongshan, E'meishan) along the northwest-trending fault in the basin. The Qishan preserves the complete stratigraphic section from Late Jurassic to Early Cretaceous among these volcanic strata. Therefore, the Qishan is the best location to investigate the volcanic lithofacies and provide direct evidence to constrain the formation age of Shoushan stone.

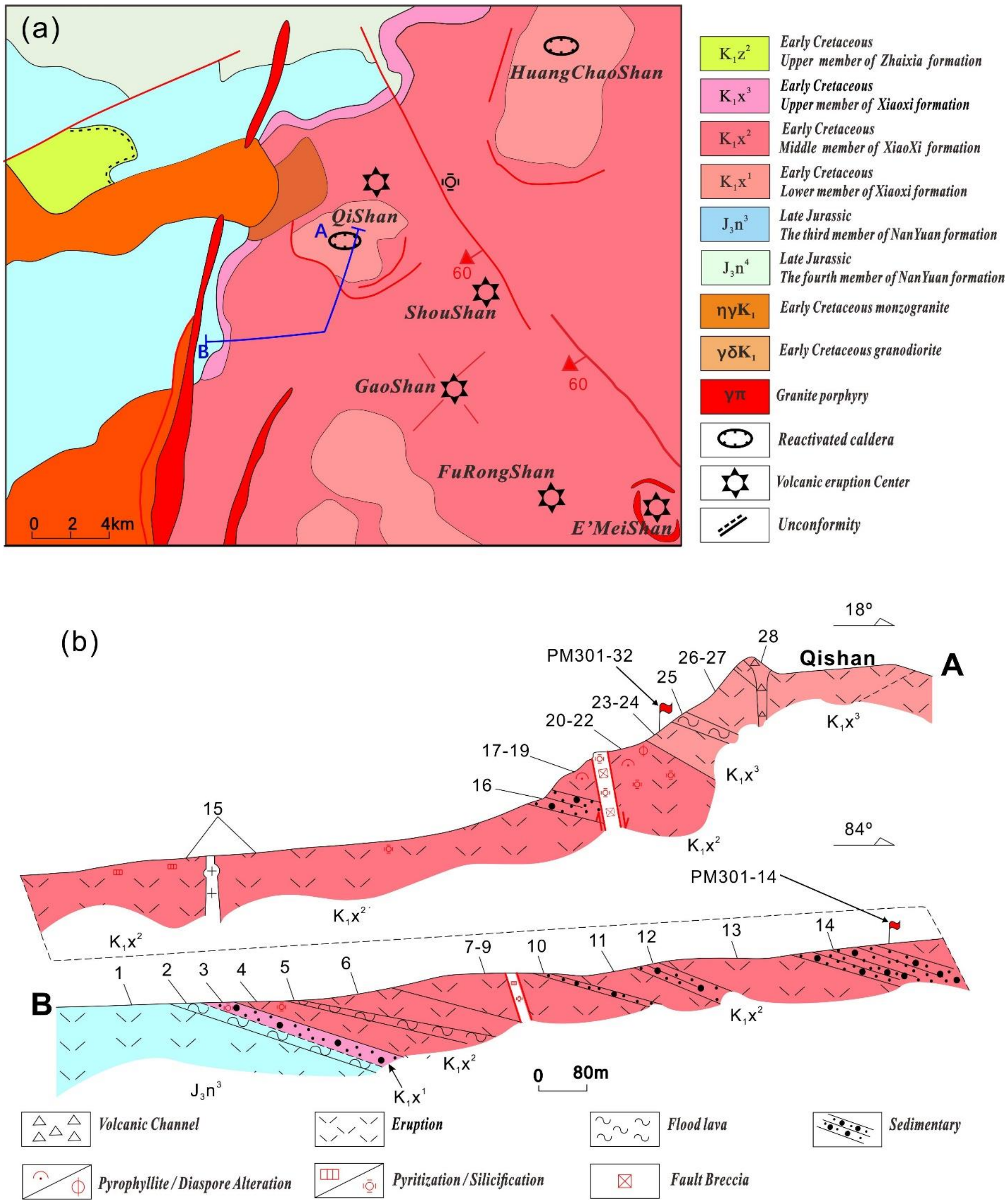


**Figure 3.** (**a**) Geologic sketch map of the northwestern Shoushan basin and investigated route of volcanic lithofacies of the Qishan caldera. (**b**) The stratigraphic section along the survey route.

## 3. Sample Description

A systematic field geological survey is carried out at the Qishan caldera along the route (A–B) shown in Figure 3. Generally, the Early Cretaceous Xiaoxi Formation is mostly composed of rhyolitic tuff and sample layers of pyrophyllite alteration (Figure 3b). The samples PM302-14 and PM302-32 (Figure 4) are collected for the geochemical character and the zircon U-Pb age analysis to obtain the upper and lower limits of magmatic-associated hydrothermal. In detail, PM302-14 (long. 119°13′36″ E, lat. 26°17′20″ N) is rhyolitic tuff with crystal debris (Figure 4d), which belongs to the middle member of the Xiaoxi Formation in the Qishan Volcanic Edifice. PM302-32 (long. 119°16′06″ E, lat. 26°18′00″ N) is rhyolitic tuff with crystal debris but from the upper member of the Xiaoxi Formation (Figure 4f). Then, PM302-24 is collected as the representative sample of alteration for research (Figure 4e). For the strong alteration and small grain size of minerals in the rock, the more lithologic characteristics of these collected samples are identified by observation of transmitted-light photomicrographs (Figure 4g–i).

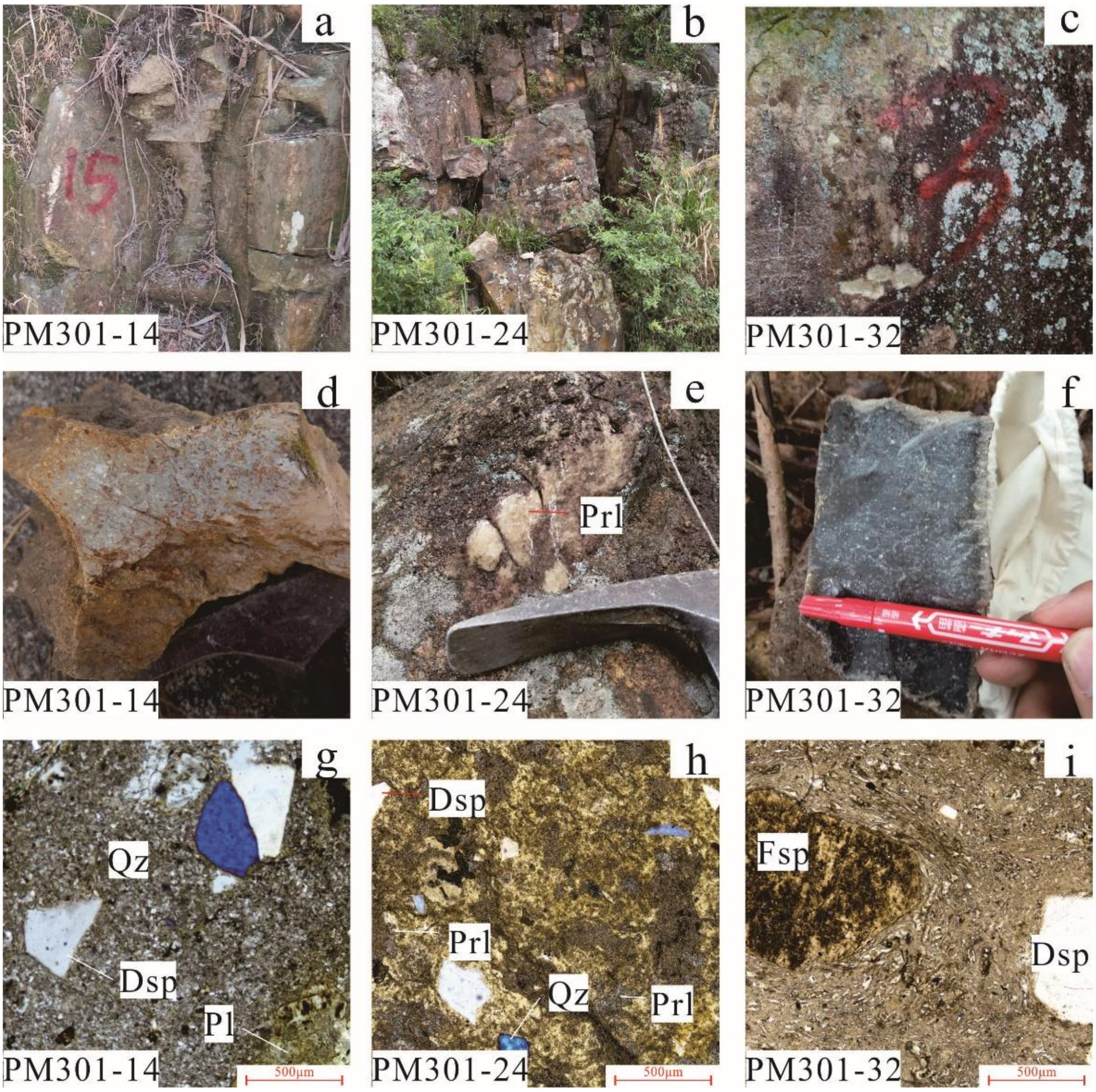


**Figure 4.** Representative photographs of unaltered rhyolitic tuff (PM302-14 and PM302-32) and rhyolitic tuff with hydrothermal alteration (PM302-24). (**a**–**c**) The outcrop in the route of geological field survey (**d**–**f**)-collected rock for geochemical analysis, (**g**–**i**); transmitted-light photomicrographs of the collected sample. Note: quartz = Qz; pyrophyllite = Prl; diaspore = Dsp; plagioclase = Pl; feldspar = Fsp.

The transmitted-light photomicrographs (Figure 4g) show that PM302-14 consists of pyroclastic materials, including crystal debris, breccia, glass debris, and felsic volcanic ash. The crystal debris consists of quartz (~5%), K-feldspar (~2%), plagioclase (~13%), and minor biotite. The transmitted-light photomicrographs (Figure 4i) demonstrate that PM302-32 also consists of pyroclastic materials and the matrix with the flow banding of crystallite. The crystal debris consists of quartz (~7%), K-feldspar (~5%), plagioclase (~3%), and minor biotite. PM302-24 is the rhyolitic tuff showing hydrothermal alteration associated with visible pyrophyllite and diaspore (Figure 4e). The transmitted-light photomicrographs show that pyrophyllite is pseudomorphic feldspar, also indicating the occurrence of hydrothermal alteration (Figure 4h). Hence, the volcanic rock of the Xiaoxi Formation is the host rock but produces Shoushan stone after hydrothermal alteration.

## 4. Analytical Methods

The collected rhyolitic tuff samples PM302-14 and PM302-32 are crushed for zircon separation and elemental analysis. In addition, rhyolitic tuff samples from the Zhouling basin collected during a previous geological survey are also sent to measure elemental composition to prospect pyrophyllite deposits. The major and trace element compositions of rhyolitic tuff from the Shoushan and Zhouling basins are all analyzed at the Geological Test Center of Fujian Province. The major elements are measured by the X-ray fluorescence spectrometer fluorescence method with an analytical error of less than 2%. The rare-earth element (REE) and trace elements are tested and analyzed by an inductively coupled plasma-mass spectrometry (ICP-MS), and the measurement accuracy is better than 5%.

The representative zircon grains of PM302-14 and PM302-32 are handpicked under a binocular microscope and mounted in epoxy resin. Then the polished zircon grains are observed and photographed under transmitted and reflected light and cathodoluminescence (CL). According to the CL image of the internal structure of zircons (Figure 5), the U-Pb ages of magmatic zircon grains are analyzed by laser ablation (LA)-ICP-MS. The zircon U-Pb geochronological analysis is conducted using an LA-ICP-MS facility housed at the State Key Laboratory of Continental Dynamics, Northwest University, Xi'an, China. An ICP-MS (Agilent 7500a) is used for the analyses involving the ablation of zircon with the GeoLas 2005 laser ablation system (wavelength of 193 nm, Lambda Physik AG, Göttingen, Germany). The laser spot diameter and frequency adopted are 32 μm and 10 Hz in this analysis.

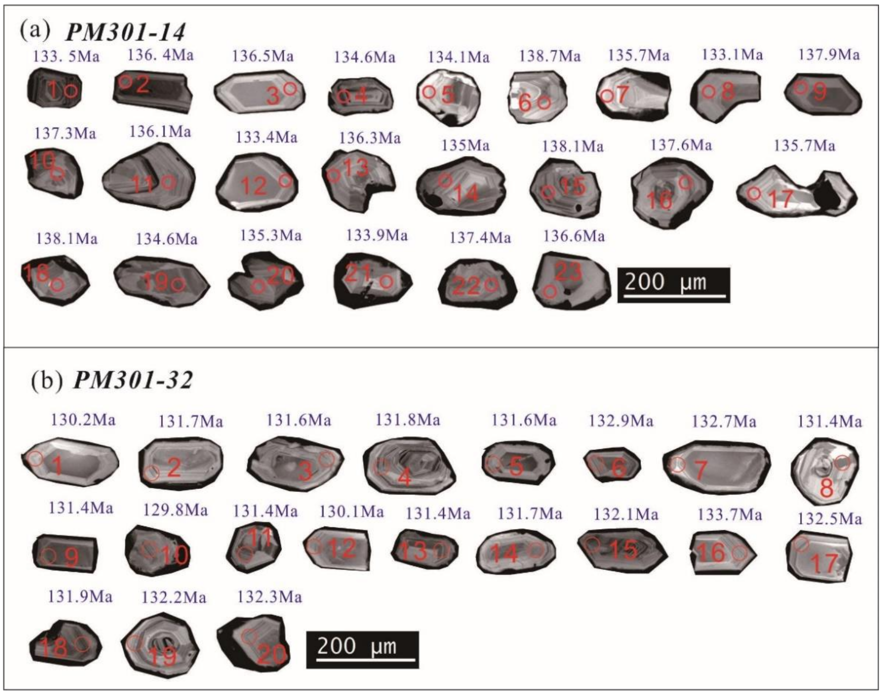


**Figure 5.** Representative zircon grains from rhyolitic tuff samples (PM302-14 and PM302-32), showing the spot location of laser ablation and $^{206}Pb/^{238}U$ apparent ages.

The zircon 91,500 is used as an external standard for calibration, and GJ-1 is adopted as an unknown sample for monitoring data quality [33]. Combined with $^{29}Si$ as internal standardization, the trace element compositions are calibrated against BCR-2G, BHVO-2G, and BIR-1G, which are the silicate reference materials produced by the United States Geological Survey (USGS). This data reduction strategy is suggested by Liu et al. [34]. All the quantitative calibrations for trace element analyses and U-Pb dating are performed by ICPMSDataCal [33,34]. The common Pb of the analytical result is corrected by the method suggested by Andersen [35].

## 5. Results and Discussion

### *5.1. Stratigraphic Section Study of the Qishan Caldera and Its Significance for the Forming of Shoushan Stone*

The geological survey and rock analysis of the Shoushan basin reveal that most volcanic eruption centers or reactivated calderas consist of middle and lower members of the Xiaoxi Formation (Figure 3). In contrast, the Qishan caldera preserves relatively complete strata from the upper to lower members, which is the best target for this stratigraphic section research. The survey route of the stratigraphic section is from the crater at the hilltop (i.e., lower member of the Xiaoxi Formation) to the parallel unconformity between rhyolite and dacite (Late Jurassic Nanyuan Formation) at the hill bottom (Figure 3b).

The total stratigraphic thickness of this section is ~1641 m, including a 44 m lower member, a 1342.6 m middle member, and a 254.4 m upper member of the Xiaoxi Formation. According to lithology, the petrogenesis of volcanic rocks is identified as the eruption facies, flood lava facies, sedimentary facies, and volcanic channel facies (Table 1). The volcanic channel facies are the crater and conduit pipe of the Qishan caldera. Eruption facies and flood lava facies record different kinds of volcanic activities. Sedimentary facies means the sedimentary rock containing volcanic ash, which may record lakes around the Qishan caldera formed by volcanic collapse. The upper member of the Xiaoxi Formation consists of the volcanic channel facies (Layer 28), the eruption facies (Layers 23, 24, 26, and 27), and the flood lava facies (Layer 25). In the middle member, the dominant layer is the eruption facies (i.e., Layers 4, 6–9, 11, 13, 15, 17–22), which is interlaced by flood lava facies (i.e., Layers 10, 12, 14, and 16) or sedimentary facies (i.e., Layer 5). The lower member is the rock of sedimentary facies (i.e., Layer 3) but with silicification. The thickest eruption facies rock in the middle member is generated by the large-scale eruption of felsic magma that would empty the underground magma chamber. It is easy to trigger large-scale caldera collapse after volcanic eruptions and form a basin for subsequent deposition, which agrees with the widespread existence of sedimentary facies. The large-scale caldera collapse also forms the system of annular and radial faults that would be the effective migration channel of hydrothermal fluid. The ore bodies of pyrophyllite or hydrothermal alteration (Layers 18–20) are controlled by these faults and distributed in arc or ring shapes around the volcanic center. There is a large-scale hydrothermal system, the heat for which would be provided by Early Cretaceous magmatism, introducing long-term alteration of some volcanic rock in the Xiaoxi Formation. Therefore, for the large-scale pyrophyllite deposit in the Shoushan basin, the hydrothermal alteration (e.g., pyrophyllite alteration, diaspore alteration, and silicification) would be essential indicators for exploration.

**Table 1.** The stratigraphic and petrogenesis result of Qishan caldera.

| Unit | Layer | Thickness (m) | Lithology Interpretation | Petrogenesis | Alteration |
|---|---|---|---|---|---|
| $K_1x^3$ | 28 | 6.7 | Rhyolitic ignimbrite with conglomerated breccia and crystal debris | Volcanic channel | - |
| | 27 | 42.6 | Rhyolitic ignimbrite with breccia and crystal debris | Eruption | - |
| | 26 | 77.9 | Rhyolitic ignimbrite with crystal debris | Eruption | - |
| | 25 | 40.8 | Lithophysa rhyolite | Flood lava | - |
| | 24 | 20.1 | Rhyolitic ignimbrite with breccia and crystal debris | Eruption | - |
| | 23 | 66.3 | Rhyolitic ignimbrite with crystal debris | Eruption | - |

**Table 1.** *Cont.*

| Unit | Layer | Thickness (m) | Lithology Interpretation | Petrogenesis | Alteration |
|---|---|---|---|---|---|
| $K_1x^2$ | 22 | 153.3 | Alterated rhyolitic tuff with crystal debris | Eruption | Diaspore and pyrophyllite alteration |
| | 21 | 24.1 | The ore body of pyrophyllite (protolith: rhyolitic tuff with crystal debris) | Eruption | Silicification, diaspore, and pyrophyllite alteration |
| | 20 | 92.2 | Alterated rhyolitic tuff with crystal-rock-vitric debris | Eruption | Pyrophyllite alteration |
| | 19 | 107.3 | Alterated rhyolitic tuff with rock-crystal debris | Eruption | Pyrophyllite alteration |
| | 18 | 21.1 | Alterated rhyolitic tuff with vitric debris | Eruption | Pyrophyllite alteration |
| | 17 | 35.8 | Rhyolitic tuff with crystal debris | Eruption | - |
| | 16 | 37.7 | Tuffaceous sandstone | Sedimentary | - |
| | 15 | 309.7 | Rhyolitic ignimbrite with crystal debris | Eruption | - |
| | 14 | 53.2 | Tuffaceous mudstone | Sedimentary | - |
| | 13 | 84.9 | Rhyolitic tuff with crystal debris | Eruption | - |
| | 12 | 30.2 | Tuffaceous mudstone | Sedimentary | - |
| | 11 | 103.3 | Rhyolitic tuff with rock debris | Eruption | - |
| | 10 | 31.5 | Tuffaceous mudstone | Sedimentary | - |
| | 9 | 20.9 | Rhyolitic tuff with breccia and crystal debris | Eruption | - |
| | 8 | 5.6 | Rhyolitic tuff with vitric debris | Eruption | Silicification and pyritization |
| | 7 | 70.3 | Rhyolitic tuff with crystal debris | Eruption | - |
| | 6 | 62.4 | Rhyolitic ignimbrite with crystal debris | Eruption | - |
| | 5 | 18.1 | Lithophysa rhyolite | Flood lava | - |
| | 4 | 81 | Silicified rhyolitic tuff with crystal debris | Eruption | Silicification |
| $K_1x^1$ | 3 | 44 | Tuffaceous mudstone with banded silicalite | Sedimentary | Silicification |
| $J_3n^3$ | 2 | 55.5 | Dacite | Flood lava | - |
| | 1 | 279 | Dacitic ignimbrite with crystal debris | Eruption | - |

### *5.2. Zircon U-Pb Geochronology of Rhyolitic Tuff in the Qishan Caldera and Its Limitation for the Forming of Shoushan Stone*

In the CL images, most prismatic grains from rhyolitic tuff in the Qishan caldera are homogeneous with oscillatory zones under fluorescence light (Figure 5), suggesting that they are possibly magmatic zircon. Twenty-three and 20 reliable U-Pb ages are obtained for the zircon grains of PM301-14 and PM301-32. All the U-Pb dating results are summarized in Table 2. The Uranium and thorium content of zircons from PM301-14 and PM301-32 are respectively in the range of 77.71–609.31 ppm (U), 11.33–410.9 ppm (Th), and 74.28–342.9 ppm (U), and 11.67–428.36 ppm (Th). The Th/U ratio of most zircons in PM301-14 and PM301-32 is more than 0.1. The U-Pb dating results of PM301-14 form a coherent group with a weighted mean $^{206}Pb/^{238}U$ age of 135.6 ± 1.0 Ma (MSWD = 0.46,

$n$ = 23) (Figure 6a,b). In contrast, 20 zircon grains from PM301-32 also give a coherent group age and yield a weighted mean $^{206}Pb/^{238}U$ age of 131.71 ± 0.86 Ma (MSWD = 0.23, $n$ = 20) (Figure 6c,d).

**Table 2.** LA-ICP-MS U-Pb analytical data for zircon from rhyolite tuff (sample PM301-14 and PM301-32) in the Shoushan volcanic basin.

| PM301-14 | | | | | | | | | | | | |
|---|---|---|---|---|---|---|---|---|---|---|---|---|
| **Analysis** | **ppm** | | **Ratios** | **Corrected Ratios** | | | | **Corrected Ages/Ma** | | | | **Concordance** |
| **No.** | **Th** | **U** | **Th/U** | **$^{207}Pb/^{235}U$** | **±1σ** | **$^{206}Pb/^{238}U$** | **±1σ** | **$^{207}Pb/^{235}U$** | **±1σ** | **$^{206}Pb/^{238}U$** | **±1σ** | |
| 1 | 11.33 | 181.51 | 0.06 | 0.14511 | 0.00495 | 0.02092 | 0.00026 | 137.6 | 4.39 | 133.5 | 1.63 | 0.97 |
| 2 | 410.9 | 609.31 | 0.67 | 0.14454 | 0.00978 | 0.02138 | 0.00038 | 137.1 | 8.67 | 136.4 | 2.37 | 0.99 |
| 3 | 93.33 | 77.58 | 1.2 | 0.14478 | 0.00882 | 0.02141 | 0.00034 | 137.3 | 7.83 | 136.5 | 2.13 | 0.99 |
| 4 | 73.19 | 89.23 | 0.82 | 0.14363 | 0.01465 | 0.02111 | 0.00046 | 136.3 | 13.01 | 134.6 | 2.89 | 0.99 |
| 5 | 127.91 | 110.98 | 1.15 | 0.14529 | 0.00788 | 0.02102 | 0.00031 | 137.7 | 6.98 | 134.1 | 1.98 | 0.97 |
| 6 | 24.47 | 68.83 | 0.36 | 0.14465 | 0.01709 | 0.02175 | 0.00058 | 137.2 | 15.16 | 138.7 | 3.68 | 1.01 |
| 7 | 214.95 | 180.46 | 1.19 | 0.14545 | 0.01083 | 0.02127 | 0.0004 | 137.9 | 9.6 | 135.7 | 2.51 | 0.98 |
| 8 | 153.84 | 177.83 | 0.87 | 0.14411 | 0.00968 | 0.02087 | 0.00036 | 136.7 | 8.59 | 133.1 | 2.3 | 0.97 |
| 9 | 452.5 | 458.37 | 0.99 | 0.14466 | 0.01827 | 0.02161 | 0.00053 | 137.2 | 16.2 | 137.9 | 3.33 | 1.01 |
| 10 | 24.93 | 71.07 | 0.35 | 0.14567 | 0.00895 | 0.02153 | 0.00035 | 138.1 | 7.93 | 137.3 | 2.2 | 0.99 |
| 11 | 11.76 | 186.93 | 0.06 | 0.14289 | 0.00708 | 0.02134 | 0.0003 | 135.6 | 6.29 | 136.1 | 1.88 | 1 |
| 12 | 196.89 | 197.47 | 1.00 | 0.14483 | 0.01081 | 0.02091 | 0.00039 | 137.3 | 9.59 | 133.4 | 2.46 | 0.97 |
| 13 | 127.74 | 128.38 | 1.00 | 0.1415 | 0.01777 | 0.02137 | 0.0006 | 134.4 | 15.81 | 136.3 | 3.78 | 1.01 |
| 14 | 23.98 | 69.14 | 0.35 | 0.14717 | 0.01517 | 0.02117 | 0.00049 | 139.4 | 13.43 | 135 | 3.09 | 0.97 |
| 15 | 59.94 | 73.84 | 0.81 | 0.14882 | 0.0134 | 0.02165 | 0.00046 | 140.9 | 11.85 | 138.1 | 2.92 | 0.98 |
| 16 | 94.21 | 110.4 | 0.85 | 0.15408 | 0.01836 | 0.02158 | 0.00058 | 145.5 | 16.15 | 137.6 | 3.65 | 0.95 |
| 17 | 99.64 | 110.65 | 0.9 | 0.14678 | 0.01342 | 0.02127 | 0.00046 | 139.1 | 11.88 | 135.7 | 2.89 | 0.98 |
| 18 | 27.28 | 77.71 | 0.35 | 0.14385 | 0.01178 | 0.02166 | 0.0004 | 136.5 | 10.46 | 138.1 | 2.51 | 1.01 |
| 19 | 12.17 | 191.66 | 0.06 | 0.14604 | 0.01065 | 0.02111 | 0.00038 | 138.4 | 9.43 | 134.6 | 2.43 | 0.97 |
| 20 | 218.96 | 185.35 | 1.18 | 0.14642 | 0.01103 | 0.02121 | 0.00041 | 138.7 | 9.77 | 135.3 | 2.6 | 0.98 |
| 21 | 173.75 | 184.65 | 0.94 | 0.14682 | 0.01087 | 0.02099 | 0.0004 | 139.1 | 9.63 | 133.9 | 2.51 | 0.96 |
| 22 | 134.27 | 128.24 | 1.05 | 0.14445 | 0.00691 | 0.02154 | 0.0003 | 137 | 6.13 | 137.4 | 1.91 | 1 |
| 23 | 153.34 | 223.17 | 0.69 | 0.14245 | 0.01605 | 0.02142 | 0.0005 | 135.2 | 14.27 | 136.6 | 3.14 | 1.01 |

| PM301-32 | | | | | | | | | | | | |
|---|---|---|---|---|---|---|---|---|---|---|---|---|
| **Analysis** | **ppm** | | **Ratios** | **Corrected Ratios** | | | | **Corrected Ages/Ma** | | | | **Concordance** |
| **No.** | **Th** | **U** | **Th/U** | **$^{207}Pb/^{235}U$** | **±1σ** | **$^{206}Pb/^{238}U$** | **±1σ** | **$^{207}Pb/^{235}U$** | **±1σ** | **$^{206}Pb/^{238}U$** | **±1σ** | |
| 1 | 208.78 | 231.94 | 0.9 | 0.14509 | 0.00864 | 0.02041 | 0.00032 | 137.6 | 7.66 | 130.2 | 2.01 | 0.95 |
| 2 | 196.59 | 261.67 | 0.75 | 0.14997 | 0.01115 | 0.02064 | 0.0004 | 141.9 | 9.84 | 131.7 | 2.53 | 0.93 |
| 3 | 249.66 | 219.96 | 1.14 | 0.13626 | 0.00591 | 0.02063 | 0.00027 | 129.7 | 5.29 | 131.6 | 1.72 | 1.01 |
| 4 | 26.7 | 75.67 | 0.35 | 0.14096 | 0.00527 | 0.02066 | 0.00026 | 133.9 | 4.69 | 131.8 | 1.64 | 0.98 |
| 5 | 327.34 | 308.56 | 1.06 | 0.13703 | 0.00684 | 0.02062 | 0.0003 | 130.4 | 6.11 | 131.6 | 1.87 | 1.01 |
| 6 | 309.17 | 282.8 | 1.09 | 0.13576 | 0.01035 | 0.02082 | 0.00036 | 129.3 | 9.25 | 132.9 | 2.3 | 1.03 |
| 7 | 169.76 | 139.39 | 1.22 | 0.13809 | 0.00807 | 0.0208 | 0.00031 | 131.3 | 7.2 | 132.7 | 1.95 | 1.01 |
| 8 | 11.67 | 183.93 | 0.06 | 0.13746 | 0.01455 | 0.02059 | 0.00044 | 130.8 | 12.99 | 131.4 | 2.81 | 1 |
| 9 | 109.8 | 86.66 | 1.27 | 0.14167 | 0.00939 | 0.0206 | 0.00035 | 134.5 | 8.35 | 131.4 | 2.19 | 0.98 |
| 10 | 138.72 | 131.56 | 1.05 | 0.13459 | 0.00621 | 0.02034 | 0.00028 | 128.2 | 5.55 | 129.8 | 1.8 | 1.01 |
| 11 | 230.15 | 241.93 | 0.95 | 0.13602 | 0.01214 | 0.02059 | 0.0004 | 129.5 | 10.85 | 131.4 | 2.54 | 1.01 |
| 12 | 25.57 | 74.28 | 0.34 | 0.14469 | 0.00697 | 0.02038 | 0.0003 | 137.2 | 6.18 | 130.1 | 1.87 | 0.95 |
| 13 | 267.9 | 304.5 | 0.88 | 0.14137 | 0.00681 | 0.0206 | 0.0003 | 134.3 | 6.06 | 131.4 | 1.88 | 0.98 |
| 14 | 219.4 | 194.08 | 1.13 | 0.13885 | 0.00708 | 0.02064 | 0.0003 | 132 | 6.31 | 131.7 | 1.87 | 1 |
| 15 | 222.5 | 228.07 | 0.98 | 0.14301 | 0.00652 | 0.0207 | 0.00029 | 135.7 | 5.8 | 132.1 | 1.81 | 0.97 |
| 16 | 81.98 | 70.12 | 1.17 | 0.13888 | 0.00822 | 0.02096 | 0.00032 | 132 | 7.33 | 133.7 | 1.99 | 1.01 |
| 17 | 192.43 | 188.87 | 1.02 | 0.14215 | 0.00665 | 0.02077 | 0.00028 | 135 | 5.91 | 132.5 | 1.8 | 0.98 |
| 18 | 201.46 | 237.43 | 0.85 | 0.14487 | 0.0082 | 0.02068 | 0.00033 | 137.4 | 7.27 | 131.9 | 2.06 | 0.96 |
| 19 | 200.06 | 244.06 | 0.82 | 0.13548 | 0.00531 | 0.02071 | 0.00026 | 129 | 4.75 | 132.2 | 1.66 | 1.02 |
| 20 | 428.36 | 342.9 | 1.25 | 0.14865 | 0.00871 | 0.02073 | 0.00034 | 140.7 | 7.7 | 132.3 | 2.17 | 0.94 |

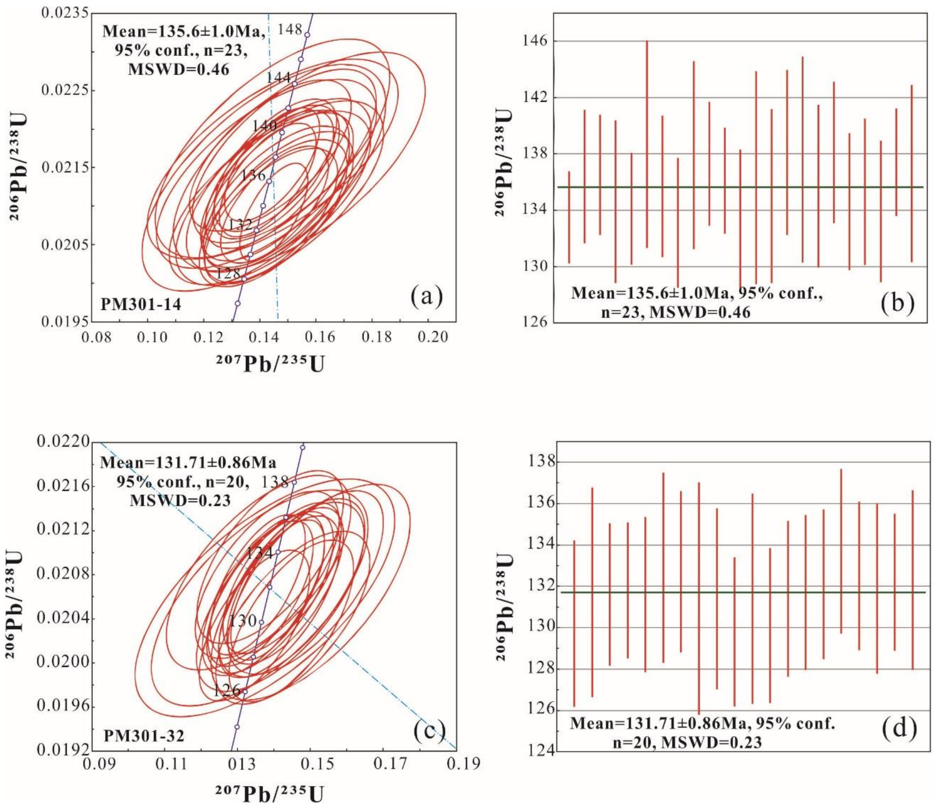


**Figure 6.** In situ analytical results of zircon U-Pb age by LA-ICP-MS, (**a**,**b**) concordia ages and their weighted average age of rhyolitic tuff sample PM302-14, (**c**,**d**) concordia ages and their weighted average age of rhyolitic tuff sample PM302-32.

Zircon U-Pb dating results demonstrated that the age range of tuff from Layer 18 to Layer 20 is later than 135.6 $\pm$ 1.0 Ma but earlier than 131.7 $\pm$ 0.9 Ma, which also limits the age of host volcanic rock for deposit. The U-Pb isotope system is known for having the highest sealing temperature, which is beneficial for dating magmatism. The sealing temperature of Pb diffusion in zircon is up to 900 °C [36,37], which is obviously higher than the temperature of epithermal hydrothermal alteration (100–405 °C). As the alteration product, the clay minerals (e.g., diaspore, pyrophyllite) will be younger than the zircons. Therefore, the hydrothermal alteration should happen in the interval time of episodic eruptions or after volcanic activity for lower temperatures. Then, the sedimentary rock containing volcanic ash (i.e., sedimentary facies) demonstrates the existence of lakes near the caldera. Combining radial faults by caldera collapse as the fluid channel, it is reasonable to assume that there has been a large-scale hydrothermal system under the caldera. Over a long-term alteration, several large-scale pyrophyllite deposits are forming in the Xiaoxi Formation. The present research is supporting that the formation of Shoushan stone is a multistage alteration process. Overall, the episodic magmatism and its interval alteration during 135–131 Ma play crucial roles in mineralization. However, the formation of high-quality Shoushan stone (i.e., filling type) still requires the continuous contribution of hydrothermal modification after volcanic activity (<131 Ma).

### *5.3. Stratigraphic Correlation of Xiaoxi Formation and Indication for Pyrophyllite Deposit Exploration*

In Fujian Province, the Xiaoxi Formation mainly occurs in a belt of volcanic basins (e.g., Shoushan, Zhouling, Liuyang, and Xiping basins) in a northeast trend, which is also named the Fu'an-Yongtai volcanic eruption belt. In this study, the stratigraphic correlation of these basins is collected and summarized in Figure 7, according to the geological survey results by the Fujian Provincial Institute of Geological Survey and Research [22,25].

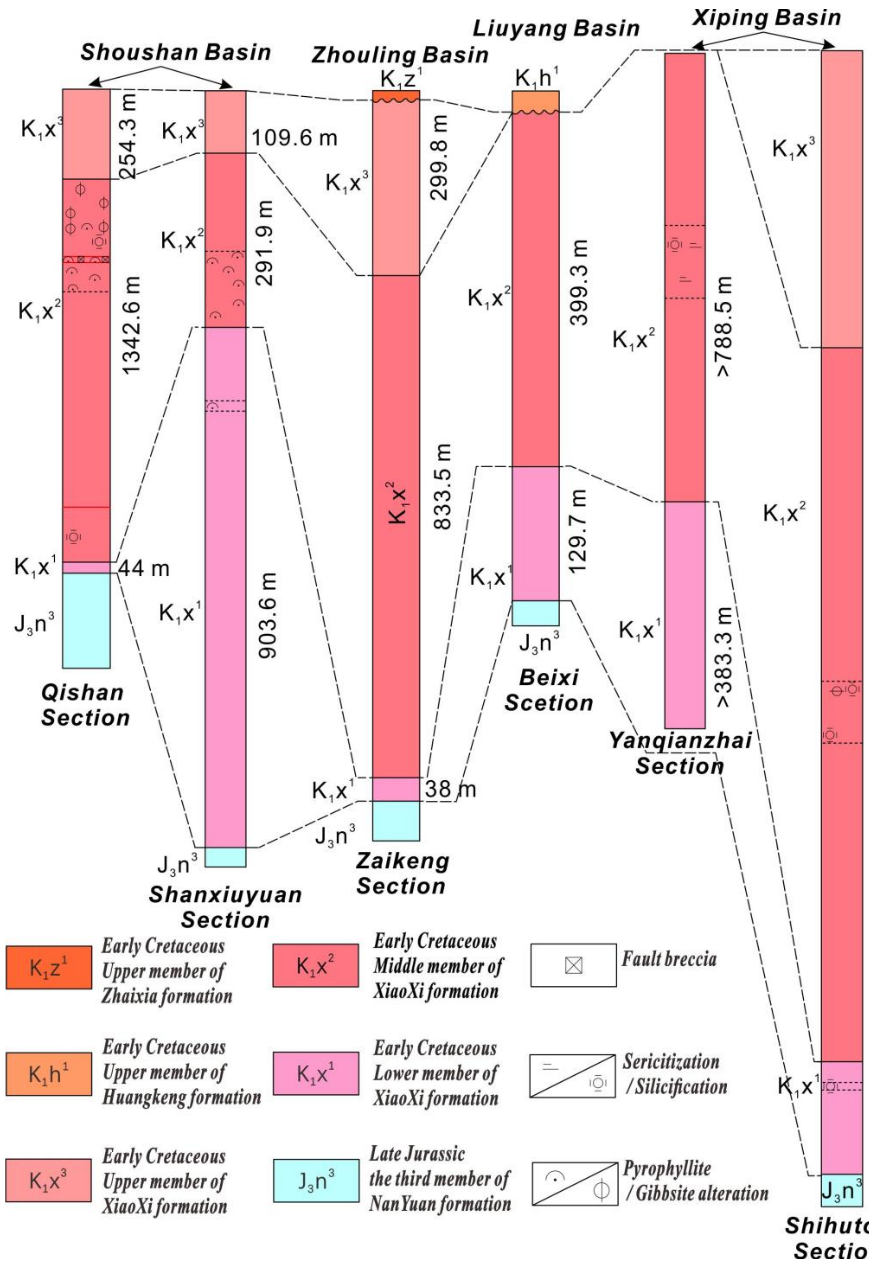


**Figure 7.** Stratigraphic correlation of Xiaoxi Formation among the sections of typical volcanic basins in Fujian Province.

The typical stratigraphic sections demonstrate the Early Cretaceous Xiaoxi Formation all overlying the Late Jurassic Nanyuan Formation in these basins. Except for the Beixi section lacking the upper member in the Liuyang basin for erosion, all the sections preserve the upper member, middle member, and lower member of the Xiaoxi Formation. The rock of eruption facies, flood lava facies, and sedimentary facies occur in the section of the Shoushan basin, Xiping basin, and Zhouling basin. In contrast, the lithofacies of rock in the Beixi section is dominantly eruption facies or flood lava facies. There is a massive variation in the thickness of the Xiaoxi Formation among these sections for the difference in volcanic regimes and magmatic intensity in the different basins. Generally, the relatively thick middle member can be observed in all basins (e.g., Shoushan basin: 1342.6 m (Qishan Section) and 291.9 m (Shanxiuyuan Section), Zhouling basin: 835.5 m (Zaikeng Section), Xiping basin: >755.5 m and 1757.5 m (Shihutou Section)). The giant eruption of magma in these basins will generate large-scale collapse that provides radial faults as the channel for hydrothermal fluid. This agrees with hydrothermal alteration layers occurring in the section of the Shoushan basin and Xiping basin. As Figure 7 shows, the Zaikeng Section indeed does not record the hydrothermal alteration, but several rock samples with pyrophyllite alteration have been found in the Zhouling basin according to the recent geological survey (unpublished). The volcanic rock in the basin is not only the host rock but also the reactant for hydrothermal alteration. Hence, we evaluate the variation in the geochemical composition between the volcanic rock of the Zhouling basin and Shoushan basin (Table 3), which is critical for further pyrophyllite deposit exploration.

Most Shoushan and Zhouling basin samples are peraluminous rhyolitic in composition (Figure 8a,b). The peraluminous and subalkaline features are beneficial for producing clay minerals with high Al content after hydrothermal alteration. On the primitive-mantle-normalized multielement diagrams (Figure 8c), there is no noticeable difference in multi-element patterns among samples from the Zhouling and Shoushan basins. Only several samples from the Zhouling basin show minor depletions of some large ion lithophile elements (LILEs, e.g., Ba and Sr) and enrichment of rare-earth elements (REE). In geochemical theory, the LILEs, Ba and Sr, can be dissolved during hydrothermal activity, which may cause the variation of these elements with strong mobility. In addition, the samples from these two basins show similar moderately steep REE patterns but significantly different Eu anomalies that may be in correlation with plagioclase. The Eu*/Eu values from the tuff of the Shoushan basin are higher than that of the Zhouling basin. This confirms that the tuff of the Shoushan basin and Zhouling basin are similar in lithology and geochemical composition. If the tuff of the Zhouling basin is altered by continuous strong hydrothermal activities, it is reasonable to form a pyrophyllite deposit containing high-quality Shoushan stone. Therefore, the Early Cretaceous Xiaoxi Formation in the Zhouling basin is an important target for future deposit explosion.

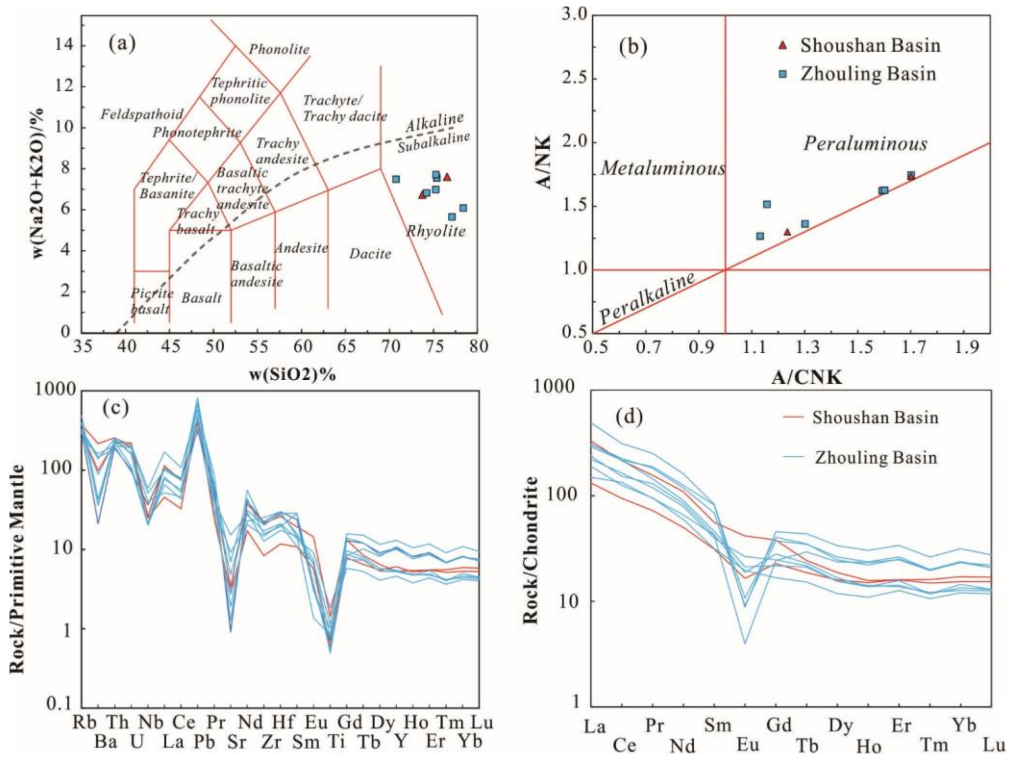


**Figure 8.** (**a**) Total alkali versus silica (TAS) classification diagram. (**b**) Molar $Al_2O_3/(CaO + Na_2O + K_2O)$ versus molar $Al_2O_3/(Na_2O + K_2O)$ diagram. (**c**) Primitive-mantle-normalized multielement patterns. (**d**) Chondrite-normalized REE patterns of volcanic rock in the Shoushan basin and Zhouling basin. The REE compositions of chondrite are from Sun and McDonough [38].

**Table 3.** Whole-rock major (wt. %) and trace element (ppm) compositions of rock samples from the Shoushan basin and Zhouling basin.

| Sample | Shoushan Basin | | Zhouling Basin | | | | | | |
|---|---|---|---|---|---|---|---|---|---|
| | PM301-14 | PM301-32 | D3185 | D3683-2 | D3691 | D3713-2 | D3713-4 | D3714 | D3712 |
| $SiO_2$ | 73.73 | 76.54 | 78.37 | 75.38 | 70.73 | 75.24 | 75.27 | 77.09 | 74.2 |
| $Al_2O_3$ | 14 | 12.56 | 11.98 | 12.88 | 14.43 | 13.79 | 12.62 | 12.76 | 13.45 |
| $Ti_2O$ | 0.31 | 0.13 | 0.16 | 0.18 | 0.26 | 0.12 | 0.23 | 0.11 | 0.19 |
| $Fe_2O_3$ | 1.71 | 0.46 | 1.06 | 1.24 | 1.36 | 1.38 | 1.36 | 1.27 | 2.2 |
| FeO | 0.27 | 0.58 | 0.3 | 0.33 | 0.74 | 0.28 | 0.24 | 0.2 | 0.56 |
| CaO | 0.09 | 0.28 | 0.08 | 0.24 | 1.62 | 0.07 | 0.65 | 0.05 | 0.11 |
| MgO | 0.37 | 0.16 | 0.14 | 0.26 | 0.4 | 0.07 | 0.24 | 0.06 | 0.1 |
| $K_2O$ | 5.37 | 5.07 | 4.69 | 5.26 | 5.01 | 5.36 | 4.85 | 5.44 | 6.25 |
| $Na_2O$ | 1.37 | 2.54 | 1.4 | 2.29 | 2.49 | 1.63 | 2.87 | 0.21 | 0.57 |
| MnO | 0.02 | 0.08 | 0.03 | 0.07 | 0.05 | 0.03 | 0.08 | 0.03 | 0.06 |
| $P_2O_5$ | 0.04 | 0.02 | 0.02 | 0.03 | 0.07 | 0.02 | 0.04 | 0.01 | 0.03 |
| LOI | 2.29 | 1.12 | 1.39 | 1.35 | 2.42 | 1.65 | 1.22 | 2.39 | 1.89 |
| Total | 99.6 | 99.6 | 99.7 | 99.5 | 99.6 | 99.7 | 99.7 | 99.6 | 99.7 |
| Cr | 3.6 | 4.5 | 4.7 | 8.5 | 6.15 | 4 | 3.7 | 2.3 | 4.9 |
| Co | 1.56 | 1.79 | 1.29 | 1.2 | 2.91 | 1.17 | 1.94 | 1.08 | 1.36 |
| Ni | 1.18 | 1.51 | 1.82 | 0.54 | 2.09 | 1.86 | 2.31 | 2.91 | 2.53 |
| V | 17.5 | 9.1 | 2.5 | 7.2 | 17.3 | 3.3 | 10.9 | 3.45 | 6.7 |
| Cu | 2.72 | 1.72 | 8.12 | 3.63 | 5.57 | 5.85 | 6.63 | 5.4 | 6.35 |
| Pb | 27.8 | 32.7 | 21.9 | 35.4 | 49.1 | 40.7 | 49.53 | 57.91 | 24.26 |
| Zn | 55.3 | 50.5 | 161.1 | 40.1 | 82.6 | 151.2 | 78.1 | 115 | 124 |
| Sn | 1.82 | 2.72 | 1.6 | 2.7 | 1.76 | 2.88 | 1.35 | 3.55 | 2.8 |
| Mo | 1.48 | 1.37 | 0.83 | 0.6 | 0.69 | 1.39 | 1.23 | 1 | 0.7 |
| Bi | 0.08 | 0.32 | 0.23 | 0.12 | 0.19 | 0.24 | 0.14 | 0.3 | 0.19 |
| W | 2.75 | 1.61 | 2.75 | 1.21 | 2.22 | 2.71 | 2.43 | 2.17 | 2.79 |
| Ag | 0.1 | 0.08 | 0.1 | 0.04 | 0.06 | 0.07 | 0.05 | 0.03 | 0.07 |
| Au | 1.28 | 0.72 | 0.54 | 1.94 | 0.52 | 0.54 | 0.52 | 0.53 | 0.52 |
| Li | 7.91 | 31.74 | 12.7 | 7.42 | 11.66 | 8.83 | 12.06 | 9.87 | 13.12 |
| Hf | 8.06 | 3.61 | 9.2 | 5.37 | 6.33 | 8.84 | 6.01 | 8.58 | 9.2 |
| Nb | 18.46 | 17.8 | 25.98 | 14.93 | 14.51 | 41.73 | 15.07 | 36.53 | 28.91 |
| Rb | 236 | 189 | 202 | 185 | 209 | 254 | 195 | 252 | 313 |
| Zr | 238 | 93.5 | 248 | 142 | 165 | 225 | 175 | 228 | 282 |
| Ti | 1858 | 779 | 926 | 1042 | 1505 | 694 | 1331 | 636 | 1100 |
| Ba | 1509 | 688 | 148 | 618 | 1018 | 257 | 972 | 248 | 300 |
| U | 4.08 | 4.61 | 2.02 | 2.31 | 2.16 | 4.32 | 3.34 | 4.1 | 3.42 |
| Th | 21.7 | 19.1 | 16.6 | 19.2 | 15.7 | 21.6 | 21.1 | 18.7 | 20.3 |
| Sr | 70.2 | 57.69 | 19.14 | 101.3 | 193.7 | 57.7 | 146.9 | 26.5 | 39.9 |
| La | 77.9 | 31.2 | 72.3 | 56.3 | 44.9 | 116 | 73.3 | 68.9 | 35.5 |
| Ce | 131 | 57.8 | 138 | 93.4 | 76.8 | 191 | 133 | 133 | 82.1 |
| Pr | 14.8 | 6.88 | 17.2 | 12.4 | 9.06 | 23.9 | 17.8 | 13.7 | 8.99 |
| Nd | 50.9 | 23.4 | 55.3 | 39.3 | 27.86 | 75.3 | 58.6 | 42.1 | 30.8 |
| Sm | 8.56 | 4.78 | 10.54 | 6.53 | 4.84 | 12.67 | 12.53 | 7.04 | 6.47 |
| Eu | 2.42 | 0.96 | 0.53 | 1.09 | 1.14 | 0.62 | 0.51 | 1.23 | 0.23 |
| Gd | 7.84 | 4.68 | 7.69 | 5.76 | 3.44 | 8.33 | 9.37 | 4.47 | 5 |
| Tb | 0.91 | 0.7 | 1.3 | 0.86 | 0.57 | 1.31 | 1.63 | 0.79 | 1.1 |
| Dy | 4.76 | 4.05 | 6.68 | 4.25 | 3.01 | 6.28 | 8.54 | 3.92 | 6.01 |
| Ho | 0.89 | 0.85 | 1.34 | 0.78 | 0.62 | 1.25 | 1.72 | 0.78 | 1.32 |
| Er | 2.64 | 2.65 | 4.36 | 2.35 | 2.1 | 4.16 | 5.62 | 2.6 | 4.1 |
| Tm | 0.38 | 0.41 | 0.51 | 0.3 | 0.27 | 0.51 | 0.67 | 0.3 | 0.5 |
| Yb | 2.61 | 2.91 | 4.04 | 2.28 | 2.05 | 3.96 | 5.36 | 2.46 | 3.97 |
| Lu | 0.39 | 0.43 | 0.53 | 0.33 | 0.3 | 0.56 | 0.7 | 0.33 | 0.53 |
| Y | 24.1 | 27.6 | 47.3 | 24.9 | 20.95 | 45.8 | 59.2 | 23.8 | 49.45 |
| Eu*/Eu | 0.9 | 0.62 | 0.18 | 0.54 | 0.85 | 0.18 | 0.14 | 0.67 | 0.12 |

## 6. Conclusions

In summary, the Qishan preserves the complete strata from Late Jurassic to Early Cretaceous in the Shoushan basin. The geological field survey identifies volcanic sequences and lithofacies of a stratigraphic section. Based on this section's result, zircon U-Pb dating results limited the age of pyrophyllite alteration during the episodic eruption. Combining the mineralization mechanism of Shoushan stone, we suggest that Shoushan stone is altered by interval hydrothermal alteration during episodic magmatism (135–131 Ma) but modified by continuous hydrothermal modification after volcanic activity (<131 Ma). The different petrogenesis demonstrates the evolution of volcanism, providing critical information for understanding the formation of Shoushan stone and its associated hydrothermal system. The stratigraphic correlation and geochemical results also allow the potential exploration of pyrophyllite deposits in other basins, according to the widespread hydrothermal alteration in the Xiaoxi Formation.

**Author Contributions:** Conceptualization, L.-Y.Z., Y.-J.L. and R.-S.C.; methodology, M.L., Z.Y. and W.X.; software, W.M. and W.X.; validation, L.-Y.Z., Y.-J.L. and M.L.; formal analysis, L.-Y.Z., W.M. and W.X.; investigation, Y.-J.L., M.L. and Z.Y.; resources, L.-Y.Z. and Y.-J.L.; data curation, L.-Y.Z., W.M. and W.X.; writing—original draft preparation, L.-Y.Z., W.M. and W.X.; writing—review and editing, Y.-J.L. and L.-Y.Z.; visualization, L.-Y.Z., W.M. and W.X.; supervision, L.-Y.Z. and R.-S.C.; project administration, L.-Y.Z. and R.-S.C.; funding acquisition, L.-Y.Z. and Y.-J.L. All authors have read and agreed to the published version of the manuscript.

**Funding:** This research is funded by the Geological Research Funding of Fujian Province ([2021]33) and National Natural Science Foundation of China (42273033 and 41803012).

**Acknowledgments:** We are grateful to three anonymous reviewers for their constructive and valuable comments, which further improved the quality of this manuscript. We acknowledge the assistance of Feng Zhao and the support from China Shoushan Stone Museum, for the photo permission of raw gemstones, arts, and crafts. We highly appreciate the suggestions of Ying Ma regarding an earlier version of this manuscript.

**Conflicts of Interest:** The authors declare no conflict of interest.

## References

1. Liu, T.-Y.; Kong, L.-L.; Lin, L.-L.; Xu, H.-D.; Zhou, Z.-Y.; Huang, M.-Z. Identifying the origins of Tianhuang stones based on Raman spectroscopy and pattern recognition algorithms. *Laser Phys.* **2022**, *32*, 045702. [CrossRef]
2. Tang, D.-P.; Wu, L.-W.; Zheng, Z.-T.; Chen, J.-L. Gemmology of some new varieties of Shoushan Stone. *J. Gems Gemol.* **2012**, *14*, 48–52.
3. Chen, T.; Yao, C.-M.; Qi, L.-J.; Tang, Y. Primary Study on Characteristics of Mineral Components and Micro-morphology of Tianhuang. *J. Gems Gemol.* **2009**, *11*, 1–5.
4. Li, Y.-J. Study on the metallogenic geological characteristics and genesis of Tianghuang from Fujian province. *J. Gems Gemol.* **2022**, *24*, 12–22.
5. Liu, Y.-G.; Chen, T. Infrared and Raman spectra study on Tianhuang. *Spectrosc. Spectr. Anal.* **2012**, *32*, 2143–2146.
6. Ren, L.-F. Mineralogy of Tianhuang gem. *Acta Petrol. Mineral.* **1988**, *7*, 151–157.
7. Tang, D.-P. Mineral components of Tianhuang and its identification. *J. Gems Gemol.* **2022**, *24*, 1–11.
8. Gan, Y.-X. *Mineralogy, Geochemistry and Genesis of Shoushan Stone Deposit*; Peking University: Beijing, China, 2001.
9. Gao, T.-J.; Zhang, Z.-L.; Liu, Z.-X. The minerogenic conditions and prospects for mineral exploration of the Shoushan Stone (Agalmatolite) in Fujian Province. *Geol. Fujian* **1997**, *16*, 110–131.
10. Li, Y.-J. On the Mineral Constituent and Characteristics of ShoushanStone. *Geol. Fujian* **2005**, *24*, 79–89.
11. Li, Y.-J.; Chen, R.-S.; Yang, Z.; Lin, M.; Wang, Y.-F.; Zhao, F. Discussion on several problems of metallogenic geological condition and genesis of Shoushan stone. *J. Gems Gemol.* **2021**, *23*, 1–11.
12. Sun, N.; Cui, W.-Y.; Xu, X. Mineralogical characteristics and genesis of Shoushan stone in Jialingshan, Fujian province. *Acta Petrol. Mineral.* **2003**, *22*, 273–278.
13. Tang, D.-P.; Zheng, Z.-T. Mineralogy and gemmology of Shoushan stone. *J. Gems Gemol.* **1999**, *1*, 28–36.
14. Wu, X.-F.; Cui, W.-Y. A mineralogical and petrographical study of Shoushan stone (Agalmatolite). *Acta Petrol. Mineral.* **1999**, *18*, 186–192.
15. Yang, Y.-X. The main mineral composition of "seal stone" is dickite mineral but not pyrophyllite mineral. *Mater. Geol.* **1995**, 8–14.
16. Zheng, J.; Chen, T.; Liu, Y.; Xu, X.; Yao, C.; Zhou, Z. Gemmological Characteristic of Jinshifeng Stone (Dickite) from Shoushan. *J. Gems Gemol.* **2022**, *24*, 43–53.

17. Mao, J.; Cheng, Y.; Chen, M.; Pirajno, F. Major types and time-space distribution of Mesozoic ore deposits in South China and their geodynamic settings. *Miner. Depos.* **2013**, *48*, 267–294.
18. Chen, R.; Zhu, L.; Jiang, S.-Y.; Ma, Y.; Hu, Q. Fluid Evolution and Scheelite Precipitation Mechanism of the Large-Scale Shangfang Quartz-Vein-Type Tungsten Deposit, South China: Constraints from Rare Earth Element (REE) Behaviour during Fluid/Rock Interaction. *J. Earth Sci.* **2020**, *31*, 635–652. [CrossRef]
19. Zhu, L.-Y.; Jiang, S.-Y.; Chen, R.-S.; Ma, Y. Origin of the Shangfang Tungsten Deposit in the Fujian Province of Southeast China: Evidence from Scheelite Sm-Nd Geochronology, H-O Isotopes and Fluid Inclusions Studies. *Minerals* **2019**, *9*, 713. [CrossRef]
20. Anovttz, L.M.; Perking, D.; Essene, E. Metastability in near-surface rocks of minerals in the system $Al_2O_3$-$SiO_2$-$H_2O$. *Clays Clay Miner.* **1991**, *39*, 225–233. [CrossRef]
21. Hemley, J.J.; Montoya, J.W.; Marinenko, J.W. Equilibria in the system $Al_2O_3$-$SiO_2$-$H_2O$ and some general implications for alteration-mineralization processes. *Econ. Geol.* **1980**, *75*, 210–228. [CrossRef]
22. Fujian Provincial Bureau of Geology and Mineral Exploration and Development. *Lithostratigraphic Cleaning in Fujian Province*; China University of Geosciences Press: Wuhan, China, 1996.
23. Lin, M. New Progress on the Study of Stratum Sequence, Rock Association and Epoch of the Xiaoxi Formation in Fujian province. *Geol. Explor.* **2011**, *47*, 555–565.
24. Lin, M. Study on the Characteristics of Volcanism of Volcanic Eruptive Basins and the Relation to Pyrophyllite Ore in Shoushan Area, Fujian Province. *Geol. Fujian* **2017**, *36*, 251–261.
25. Fujian Provincial Bureau of Geology and Mineral Exploration and Development. *Regional Geology of Fujian Province*; Geological Publishing House: Beijing, China, 1985.
26. Charvet, J. The Neoproterozoic-Early Paleozoic tectonic evolution of the South China Block: An overview. *J. Asian Earth Sci.* **2013**, *74*, 198–209. [CrossRef]
27. Zhao, J.-H.; Zhou, M.-F.; Yan, D.-P.; Zheng, J.-P.; Li, J.-W. Reappraisal of the ages of Neoproterozoic strata in South China: No connection with the Grenvillian orogeny. *Geology* **2011**, *39*, 299–302. [CrossRef]
28. Li, X.-H.; Li, W.-X.; Li, Z.-X.; Lo, C.-H.; Wang, J.; Ye, M.-F.; Yang, Y.-H. Amalgamation between the Yangtze and Cathaysia Blocks in South China: Constraints from SHRIMP U-Pb zircon ages, geochemistry and Nd-Hf isotopes of the Shuangxiwu volcanic rocks. *Precambrian Res.* **2009**, *174*, 117–128. [CrossRef]
29. Zhou, X.-M.; Sun, T.; Shen, W.-Z.; Shu, L.-S.; Niu, Y.-L. Petrogenesis of Mesozoic granitoids and volcanic rocks in South China: A response to tectonic evolution. *Episodes* **2006**, *29*, 26–33. [CrossRef] [PubMed]
30. Li, Z.-X.; Li, X.-H. Formation of the 1300-km-wide intracontinental orogen and post-orogenic magmatic province in Mesozoic South China: A flat-slab subduction model. *Geology* **2007**, *35*, 179–182. [CrossRef]
31. Zhou, X.-M.; Li, W.-X. Origin of Late Mesozoic igneous rocks in Southeastern China: Implications for lithosphere subduction and underplating of mafic magmas. *Tectonophysics* **2000**, *326*, 269–287. [CrossRef]
32. Yu, M.-G.; Hong, W.-T.; Yang, Z.-L.; Duan, Z.; Chu, P.-L.; Chen, R.; Cao, M.-X. Classification of Yanshanian volcanic cycle and the related mineralization in the coastal area of southeastern China. *Geol. Bull. China* **2021**, *40*, 845–863.
33. Liu, Y.-S.; Gao, S.; Hu, Z.-C.; Gao, C.-G.; Zong, K.-Q.; Wang, D.-B. Continental and oceanic crust recycling-induced melt-peridotite interactions in the Trans-North China Orogen: U-Pb dating, Hf isotopes and trace elements in zircons from mantle xenoliths. *J. Petrol.* **2010**, *51*, 537–571. [CrossRef]
34. Liu, Y.-S.; Hu, Z.-C.; Gao, S.; Günther, D.; Xu, J.; Gao, C.-G.; Chen, H.-H. In situ analysis of major and trace elements of anhydrous minerals by LA-ICP-MS without applying an internal standard. *Chem. Geol.* **2008**, *257*, 34–43. [CrossRef]
35. Andersen, T. Correction of common lead in U-Pb analyses that do not report 204Pb. *Chem. Geol.* **2002**, *192*, 59–79. [CrossRef]
36. Cherniak, D.J.; Watson, E.B. Pb diffusion in zircon. *Chem. Geol.* **2001**, *172*, 5–24. [CrossRef]
37. Lee, J.K.W.; Williams, I.S.; Ellis, D.J. Pb, U and Th diffusion in natural zircon. *Nature* **1997**, *390*, 159–162. [CrossRef]
38. Sun, S.S.; McDonough, W.F. Chemical and isotopic systematics of oceanic basalts: Implications for mantle composition and processes. In *Magmatism in the Ocean Basin*; Geological Society Special Publication: London, UK, 1989; Volume 42, pp. 313–345.